Catalysis Today 143 (2009) 225–229

Contents lists available at ScienceDirect

Catalysis Today

journal homepage: www.elsevier.com/locate/cattod

Visualization of the three-dimensional microstructure of TiO_2 nanotubes by electron tomography

A.B. Hungría *, D. Eder, A.H. Windle, P.A. Midgley

Department of Materials Science and Metallurgy, University of Cambridge, Pembroke Street, Cambridge CB2 3QZ, UK

ARTICLE INFO

Article history:
Available online 5 November 2008

Keywords:
Rutile nanotubes
Electron tomography
STEM–HAADF imaging
TiO_2

ABSTRACT

The internal microstructure of pure rutile nanotubes has been elucidated by means of high angle annular dark field scanning transmission electron tomography. The formation and stability of pure rutile fully hollow nanotubes, after removal of carbon nanotubes used as templates is confirmed by 3D electron tomogram analysis. The size, shape and distribution of the nanocrystals which constitute the nanotube, are also characterized by tomography.

1. Introduction

For many years titanium oxide (TiO_2) has been one of the most investigated transition metal oxides, owing to its importance and potential in many fields, and in particular those related with photocatalysis [1,2] and environmental catalysis [3,4]. One way of improving the properties of TiO_2-based catalysts is by designing nanostructured mechanically coherent architectures, as nanotubes or nanofibrils, which can provide ready gas access to high surface area [5,6]. Nanotubes made of inorganic oxides such as SiO_2, Al_2O_3, V_2O_5, MoO_3 and TiO_2 have been synthesized employing different methodologies such as self-assembly or through the use of carbon nanotubes as templates [5]. In the particular case of TiO_2, anatase or TiO_x polymorph nanotubes have been synthesized and used in applications [7]. An important advance however is to prepare pure rutile nanotubes which are expected to have a higher selectivity and improved kinetics in photo-catalytic reactions [8,9] as well as a better performance in other catalytic reactions as hydrogen production from biomass [10], the oxidation of aromatic hydrocarbons [11] and the dissociative adsorption of H_2S [12].

The present work focuses on the three-dimensional characterization of pure rutile nanotubes by means of electron tomography prepared for the first time by a sol–gel route using multi-wall carbon nanotubes as sacrificial templates [6]. High angle annular dark field (HAADF), scanning transmission electron microscopy (STEM) tomography [13] has already been applied successfully in the study of field of heterogeneous catalysis to investigate the spatial distribution and morphology of supported nanoparticles [14,15] and oxide nanoparticles used as support [16]. This technique is indeed extremely valuable to characterize systems where, as in the case of nanotubes, it is important not only to know the three-dimensional external morphology of the sample but also the knowledge of its inner structure [17]. The information provided by electron tomography at different stages of the growth process will enable us to confirm whether TiO_2 nanotubes are formed; this is particularly important in the last step of the synthesis, when the carbon nanotube used as a template should be removed to give rise to separate rutile nanotubes. Awareness of the microstructure is of great importance in understanding what processes control the properties of rutile nanotubes, compared with conventional rutile nanocrystalline samples.

2. Experimental

Samples were synthesized as described elsewhere [6] by a sol–gel route using benzyl alcohol as surfactant and carbon nanotubes as templates, with subsequent heat treatment used to convert the templated near-amorphous titania first to anatase and then to rutile. The process can be described briefly as follows: after coating the carbon nanotubes with near-amorphous titania through the sol–gel process, the sample is heated in air to produce anatase (sample CNT_A). This is then heated in nitrogen to transform most of the anatase to rutile (sample CNT_A + R) and finally heated in air again, but at a higher temperature, to burn off the carbon nanotube and to transform any remaining anatase to rutile (sample R). Initial analysis of the phases present in each sample after the consecutive treatments was performed by means of XRD and electron diffraction [6,18].

* Corresponding author. Current Address: University of Cadiz, Spain. Tel.: +34 646 960325.
E-mail address: ana.hungria@uca.es (A.B. Hungría).

0920-5861/$ – see front matter © 2008 Elsevier B.V. All rights reserved.
doi:10.1016/j.cattod.2008.09.014

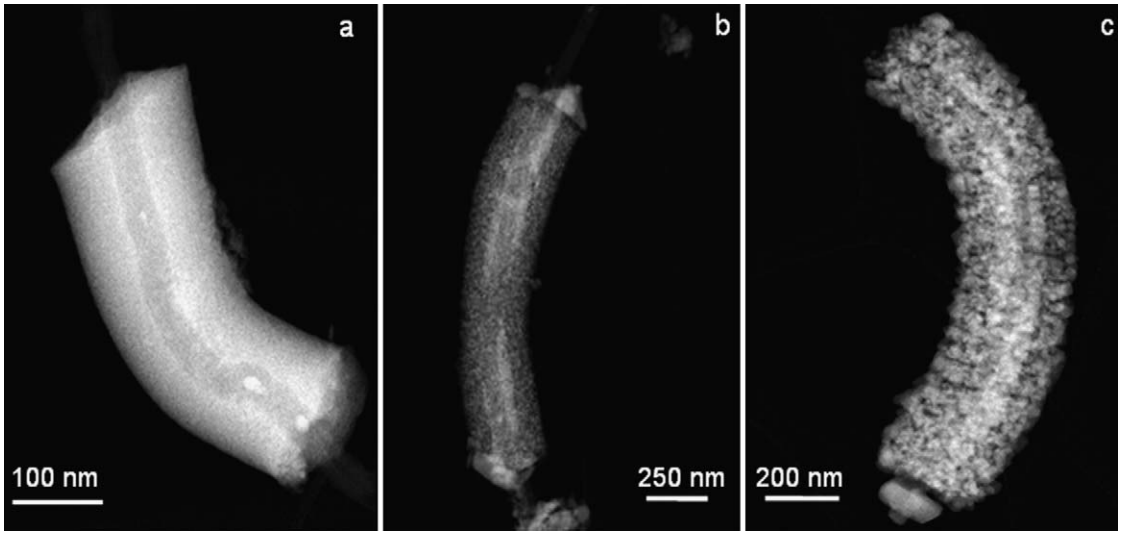

Fig. 1. HAADF–STEM images of (a) sample CNT_A with a carbon nanotube and as-deposited anatase, (b) sample CNT_A + R with carbon nanotube and a mix of anatase and (c) sample R composed of only rutile.

HAADF–STEM images were acquired on a FEI Tecnai F20 field emission gun transmission electron microscope operated at 200 kV. For the tomography studies, on CNT_A, CNT_A + R and R samples, a single tilt series of HAADF–STEM images was recorded over a wide angular range every 2° using a Fischione ultrahigh-tilt tomography holder. The minimum and maximum tilt angle image acquired without specimen self-shadowing for each sample was: −76° and +70° for CNT_A, −70° to +72° for CNT_A + R and from −74° to +74° for R.

Image acquisition was undertaken using the FEI software package Xplore3D. Images were then aligned sequentially using Inspect 3D. Reconstructions were performed with Inspect 3D.

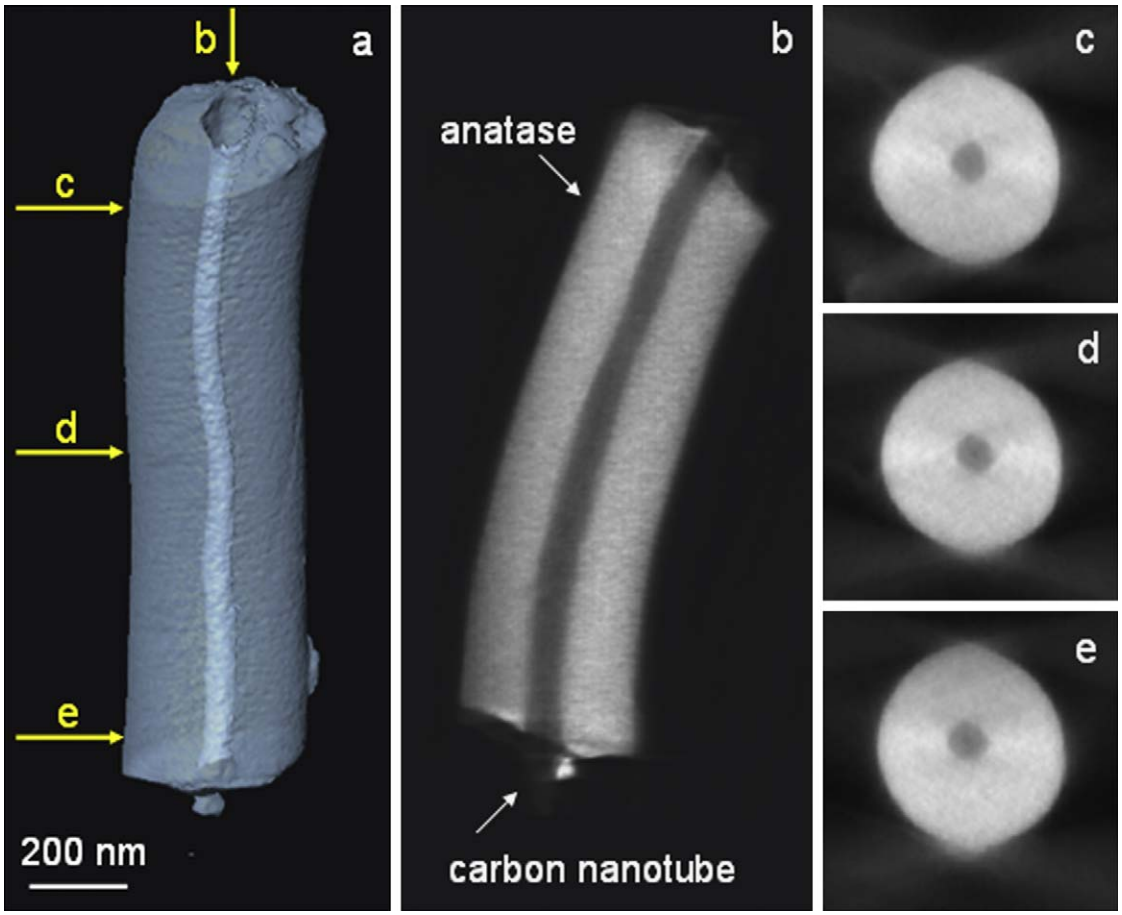

Fig. 2. (a) Semi-transparent surface render of a reconstruction of sample CNT_A showing only the as-deposited anatase. (b) Longitudinal slice and (c–e) axial slices through the reconstruction. The positions of slices (b–e) are marked in (a). See Supporting Information for a video of the full dynamic tomogram.

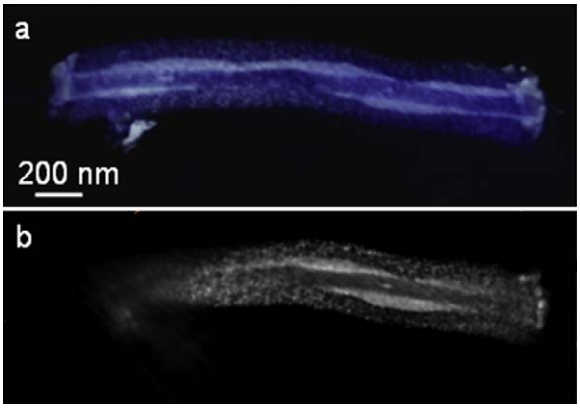

Fig. 3. (a) Voxel projection of the tomographic reconstruction of sample CNT_A + R; (b) a longitudinal slice through the centre of the reconstructed tomogram. The formation of an inner layer close to the carbon nanotube is evident.

Weighted back-projection (WBP) routine was used to test the goodness of the alignments. Final reconstructions were performed with simultaneous iterative reconstruction technique (SIRT) which constrains the reconstructed volume to best match the original images when re-projected back along the original tilt directions. This constraint has the effect of minimizing some of the unwanted effects of the limited data sampling and greatly reduces the "fan" artefact that can be evident in many WBP reconstructions. Voxel projections were constructed in Inspect 3D, and surface rendering (after a segmentation process when needed) was undertaken using Amira software.

3. Results and discussion

Fig. 1 shows representative STEM–HAADF images of samples (a) CNT_A, (b) CNT_A + R and (c) R. In these images the nanotube morphology is apparent but details are obscured by the projection effect. The samples are polycrystalline, the nanotubular form being produced by an aggregation of nano-crystallites. As the intensity of HAADF–STEM images is approximately proportional to the square of the atomic number Z [19], there is a large difference between the intensity in the image of the carbon nanotube and the titania; the carbon nanotube is in fact barely visible in samples CNT_A and CNT_A + R shown in Fig. 1(a) and (b), respectively. No features corresponding to carbon nanotubes were found in any of the images recorded for sample R (Fig. 1(c)).

HAADF–STEM tomography studies were performed to characterize in three dimensions the samples at the different stages of the synthesis. Fig. 2(a) shows a semi-transparent surface render of the CNT_A sample tomogram, together with (b) a longitudinal and (c)–(e) axial slices through the reconstructed tomogram. The tomographic reconstruction shows a nanotube with an apparently near-homogeneous surface and interior where individual anatase nanoparticles cannot be resolved. It should be noted that reconstruction resolution scales with the size of the overall object. Fig. 2(b) corresponds to a longitudinal slice containing the tube axis; the carbon nanotube with far lower intensity can just be

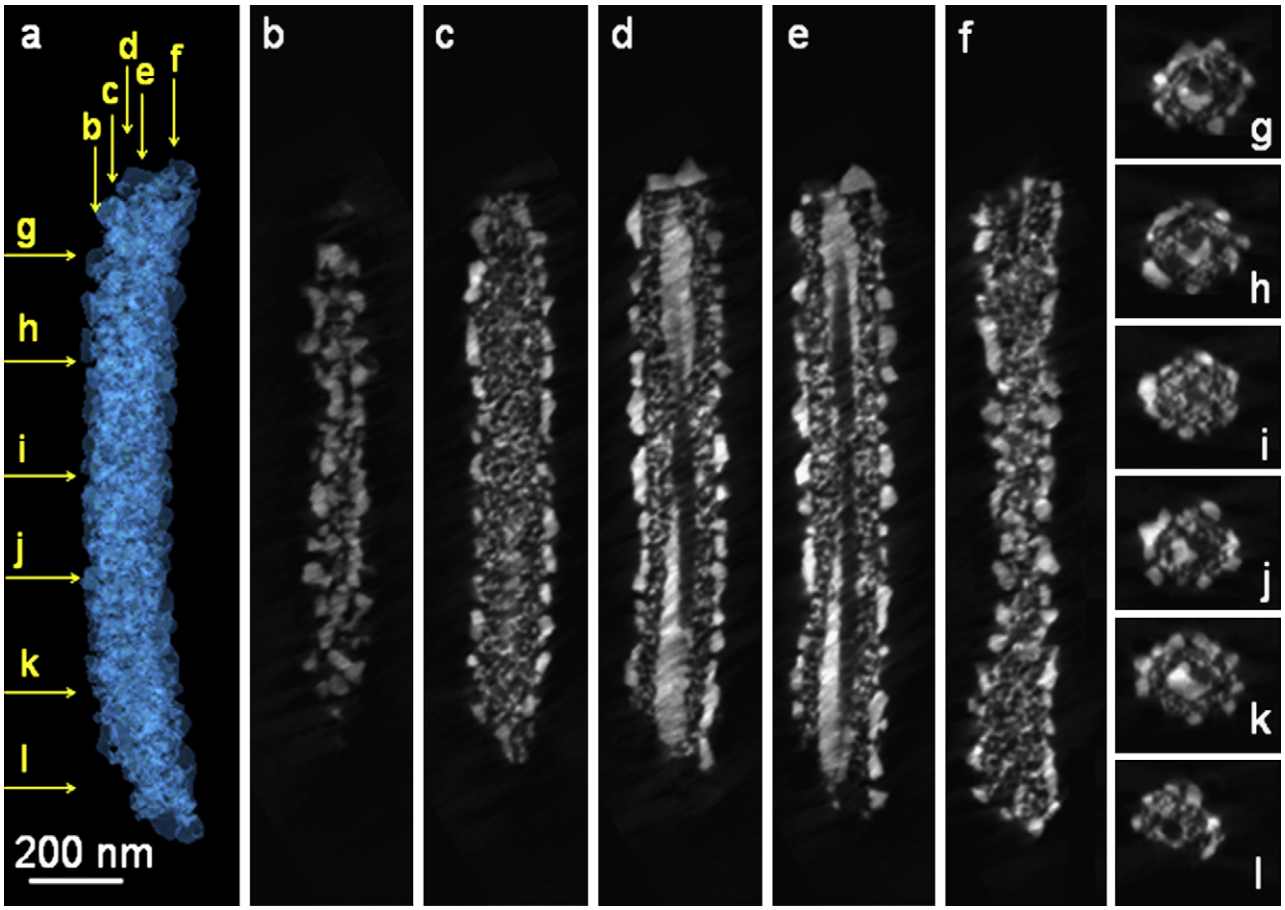

Fig. 4. (a) Voxel projection of the tomographic reconstruction of sample R. (b–f) A series of individual slices through the reconstructed nanotube in a direction parallel to the axis and (g–l) a series of slices in a direction perpendicular to the nanotube axis. The position of the individual slices is indicated with arrows in (a). See Supporting Information for a video of the full dynamic tomogram.

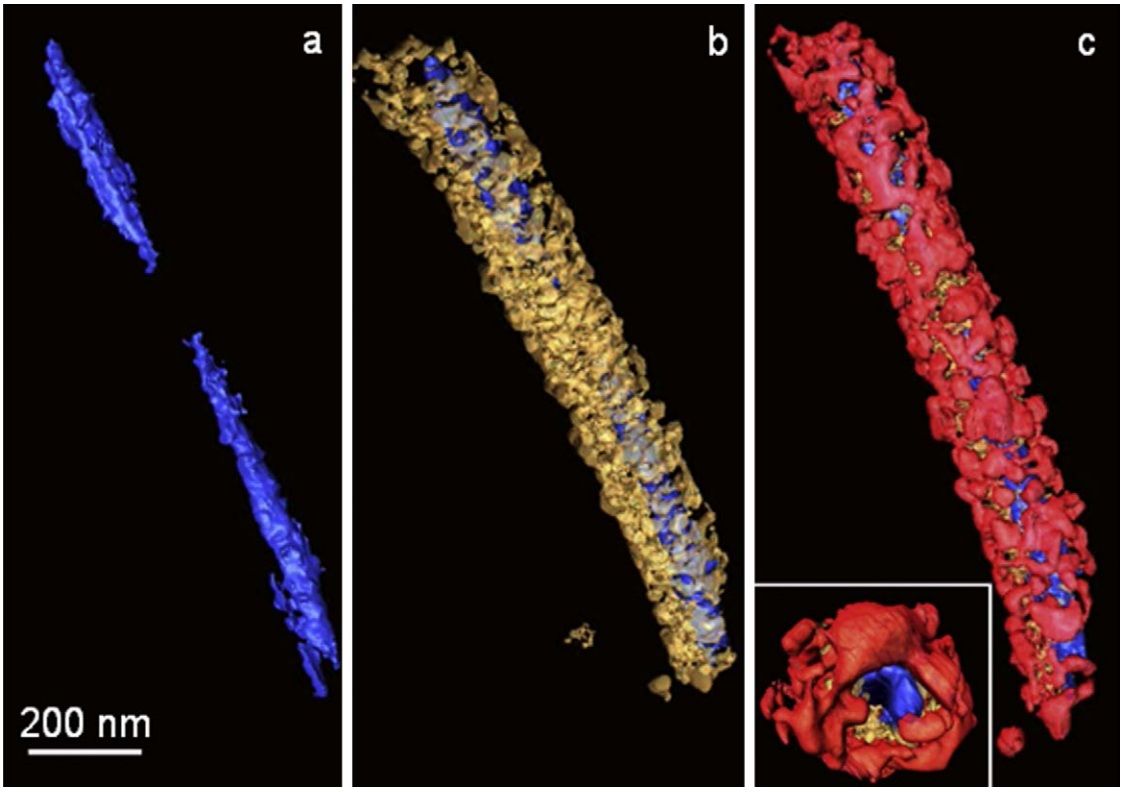

Fig. 5. Surface renders of the reconstructed volume after segmentation of the particles with different morphology. (a) Shows the inner layer, (b) small particles surrounding the inner layer and the complete segmented rutile nanotube is shown in (c) with a projection perpendicular to the axis displayed in the inset (at twice the magnification of the main image). See Supporting Information for a video of the full dynamic tomogram.

distinguished from the anatase layer. The continuity and homogeneity of the anatase layer can be confirmed by observing axial slices perpendicular to the tube axis in Fig. 2(c–e). In sample CNT_A + R, after most of the anatase has been transformed to rutile, the analysis performed by electron tomography reveals that the titania layer composed of a mix of anatase and rutile is far from homogeneous. Fig. 3(a) shows a voxel projection of the reconstructed tomogram where some individual particles can be resolved. In this projection, and in the longitudinal slice through the tomogram depicted in Fig. 3(b), it is clear that there is a region, located at the interface between the carbon nanotube and the anatase + rutile layer, where the particles seem to have sintered and ripened, forming a continuous layer at the interface.

Sample R was studied by electron tomography, not only to confirm, as previously mentioned, the fidelity of the titania nanotube structure after removal of the carbon nanotube, but also to examine the internal structure of the region close to the tube axis after the complete transformation of anatase to rutile. Fig. 4 displays (a) a voxel projection of the tomographic reconstruction together with a series of slices through the nanotube (b–f) in a direction parallel to the tube axis, and (g–l) in a direction perpendicular to it. From the observation of the slices displayed in Fig. 4(b–f) it is evident that there is significant variation in particle size which is dependant on the distance from the nanotube axis. Particles located on the surface of the nanotube are larger in diameter (ca. 50–60 nm) compared with particles inside (ca. 10 nm), see Fig. 4(b) and (c). In addition, the solid continuous inner layer close to the axis of the nanotube, present in sample CNT_A + R, is also present in sample R and to a greater extent; the continuous layer is visible along the full tube length, see Fig. 4(d) and (e). The origin of this inner layer is not certain, but is likely to be related to the constrained geometry of the nanotube. On the surface, rutile crystals have sufficient freedom to develop and grow separately. At the inner surface of the nanotube, the high curvature and the restrictive volume might encourage the crystals to coalesce as they grow. In addition, factors such as the relatively high thermal conductivity of the carbon nanotube [20] which will affect the heating rate of the regions in direct contact with the carbon nanotube, or a possible chemical interaction between the anatase crystals with the outer layer of the carbon nanotube, may be responsible for the formation of the solid inner layer.

Slices perpendicular to the tube axis displayed in Fig. 4(g–l) clearly show the different particles size and morphology depending on their proximity to the surface; the cross-section of the inner layer can also be seen clearly. The slices displayed in Fig. 4 (g–l) confirm the structural fidelity of the rutile nanotube structure following the removal of the carbon nanotube. They also indicate an apparent partial filling of the central axial void, after the removal of the carbon nanotube, by the inner layer of rutile. Fig. 5 shows the projection of the reconstructed volume after manual segmentation. The segmentation process enables the reconstruction to be divided into different sub-volumes depending on the particle sizes analyzed in Fig. 4. Fig. 5(a) shows the inner layer, the small particles surrounding the inner layer are displayed in Fig. 5(b) and the overall segmented nanotube is shown in Fig. 5(c). The inset of Fig. 5(c) shows a projection of the segmented structure in a direction perpendicular to the nanotube axis.

4. Conclusions

The complex three-dimensional structure of rutile nanotubes has been elucidated by means of STEM–HAADF electron tomo-

graphy. The reconstructed volumes can be manipulated in order to study both the internal and the external structure of the objects, retrieving unique information at a nanometric scale. The three-dimensional analysis confirms the formation of pure rutile nanotubes composed of particles of different sizes depending on their position with respect to the tube axis. This information is very important to understand the physical and chemical properties of rutile nanotubes compared with rutile powders.

Acknowledgments

A.B.H. thanks the European Community for a Marie Curie Research Fellowship and D.E. thanks the Austria Academy of Science for a APART fellowship. P.A.M. thanks the Isaac Newton Trust for funding. The authors acknowledge financial support from the European Union under the Framework 6 program for an Integrated Infrastructure Initiative, Ref.: 026019 ESTEEM.

Appendix A. Supplementary data

Supplementary data associated with this article can be found, in the online version, at doi:10.1016/j.cattod.2008.09.014.

References

[1] A.L. Linsebigler, L. Guanquan, J.Y. Yates, Chem. Rev. 95 (1995) 735.
[2] M.R. Hoffmann, S.T. Martin, W. Choi, D.W. Bahnemannt, Chem. Rev. 95 (1995) 69.
[3] M. Haruta, S. Tsubota, T. Kobayashi, H. Kageyama, M.J. Genet, B. Delmon, J. Catal. 144 (1993) 175.
[4] M. Valden, X. Lai, D.W. Goodman, Science 281 (1998) 1647.
[5] C.N.R. Rao, M. Nash, Dalton Trans. 1 (2003) 1.
[6] D. Eder, I.A. Kinloch, A.H. Windle, Chem. Commun. (2006) 1478.
[7] O.K. Varghese, D. Gong, M. Paulose, K.G. Ong, E.C. Dickey, C.A. Grimes, Adv. Mater. 15 (2003) 624.
[8] O. Carp, C.L. Huisman, A. Reller, Prog. Solid State Chem. 32 (2004) 33.
[9] A.R. Grandhe, J.B. Fernandes, S. Varma, N.M. Gurpa, J. Mol. Catal. A: Chem. 238 (2005) 63.
[10] H.-S. Roh, D.L. King, Y. Wang, Prepr. Am. Chem. Soc., Div. Pet. Chem. 49 (2004) 2.
[11] S.C. Kim, J. Hazard. Mater. 91 (2002) 285.
[12] D.D. Beck, R.W. Siegel, J. Mater. Res. 7 (1992) 2840.
[13] P.A. Midgley, M. Weyland, Ultramicroscopy 96 (2003) 413.
[14] P.A. Midgley, M. Weyland, J.M. Thomas, P.L. Gai, E.D. Boyes, Angew. Chem. 41 (2002) 3804.
[15] H. Friedrich, J.R.A. Sietsma, P.E. de Jongh, A.J. Verkleij, K.P. de Jong, J. Am. Chem. Soc. 129 (2007) 10249.
[16] J.C. Hernandez, A.B. Hungria, J.A. Perez-Omil, S. Trasobares, S. Bernal, P.A. Midgley, A. Alavi, J.J. Calvino, J. Phys. Chem. C 111 (2007) 9001.
[17] O. Ersen, J. Werckmann, M. Houlle, M.J. Ledoux, C. Pham-Huu, Nano Lett. 7 (2007) (1898).
[18] D. Eder, A.H. Windle, J. Mater. Chem. 18 (17) (2008) 2036.
[19] M.M.J. Treacy, A. Howie, J. Catal. 63 (1980) 265.
[20] E.T. Thostensona, Z. Renb, T.-W. Choua, Compos. Sci. Technol. 61 (2001) 1899.